Instituto Tecnológico y de Estudios Superiores de Monterrey

Campus Monterrey

School of Engineering and Sciences

Adsorption Mechanisms of Glycine onto Graphene Oxide Models: A Computational Approach from DFT and AIMD Simulations

A thesis presented by

Fausto Guilherme Abril Martínez

Submitted to the
School of Engineering and Sciences
in partial fulfillment of the requirements for the degree of

Master of Science
In
Nanotechnology

Monterrey Nuevo León, December 03th, 2021

Index

Summary 7
1. Introduction 11
2. Background 15
   2.1 Carbon nanotechnology 15
   2.2 Density functional theory (DFT) 17
   2.3 Exchange correlation functional 19
   2.4 Basis set 21
   2.5 Dispersion correction 22
   2.6 Geometry optimization 23
   2.7 Conductor-like Polarizable Continuum Model (CPCM) 23
   2.8 Ab initio molecular dynamics (AIMD) 24
3. Hypothesis and objective 25
4. Methodology 26
5. Results and discussion 29
   5.1 Optimized structures 29
   5.2 Electronic properties 34
   5.3 Interaction energy 36
   5.4 Thermodynamic stability 38
   5.5 Comparison with other models 43
6. Conclusion 45
7. Outlook 46
8. Bibliography 47
9. Supplementary information 52

Dedication

To my wife and my parents who encouraged me in this journey through the nanotechnology realm.

Acknowledgments

I would like to thank Consejo Nacional de Ciencia y Tecnología (CONACyT) for the financial support provided (CVU: 1035162) and Tecnológico de Monterrey for the scholarship that has gave me the opportunity to follow this master's program.

I want to say many thanks to my thesis supervisor, Dr. Flavio Fernando Contreras Torres, for his encouragement and support in my education. His vitality and interest inspired me to explore the realm of computational physics and chemistry. I have been honored with the opportunity to work with him on this project.

I would also like to thank my committee members Dr. Jorge Luis Cholula Díaz, Dr. Servando López Aguayo, and Dr. Héctor Javier Medel Cobaxin, for their support, guidance, for their invaluable time and insightful comments during the realization of this thesis.

Finally, I want to thank all the members of the Laboratorio de Nano y Microestructuras for all their support.

Adsorption Mechanisms of Glycine onto Graphene Oxide Models: A Computational Approach from DFT and AIMD Simulations

by

Fausto Guilherme Abril Martínez

Summary

Nanomedicine is a nanotechnology application based on the engineering of nanomaterials to develop tools for diagnosis, prevention, imaging, and treatment of diseases. Understanding the interaction mechanisms between nanomaterials and biomolecules is essential in creating novel sensing platforms such as electrochemical devices, drug delivery systems, and biosensors. Carbon has become the most widely used nanomaterial in the 21st century. Graphene (G) is the most important allotrope because of its intrinsic properties, such as a zero bandgap. However, due to the sophisticated synthesis procedures, several related G materials are proposed to be used in applications. Graphene oxide (GO) contains oxidized functional groups on the surface, which can serve to functionalize with other molecules and thus enhance the chemical and physical properties as compared to graphene. Moreover, structural defects can appear in both G and GO materials which are also influenced by the properties of these materials. G and GO can have a perfect lattice or contain Stone-Wales structural defects that are formed by rotating a C-C bond 90º, which creates a 5-7 ring pair.

The investigation of interactions of important biomolecules with carbon-based nanomaterials (CNMs) has emerged in an explosion of research since CNMs are extensively proposed for biological assays to detect biomarkers facilitating their detection and optical imaging in biological systems. In this way, amino acids (AAs) are the critical chemical structures in organisms. AAs are

known as the building blocks of proteins. AAs can manifest the common physical-chemical properties of more significant biomolecules. Glycine (GLY) is the simplest amino acid; therefore can serve as a simple novel to evaluate this amino acid's adsorption process in CNMs. A first approximation of the interaction mechanism between G (or GO) with GLY can be studied at a fundamental level using theoretical approaches.

Density functional theory (DFT) and Ab-initio molecular dynamics (AIMD) are modern tools to gain insights into the interaction mechanisms and microscopic details of chemical processes in both gas-phase and solvent medium (e.g., water). DFT is a set of quantum mechanical approaches to investigate the electronic structure of a system at its ground state. However, DFT is not accurate for accounting for noncovalent intermolecular interactions, and they can be described using semi-empirical approaches. Atom-pairwise specific dispersion coefficients ($-C_6/R^6$) and cutoff radii that are both computed from time-dependent first principles have proved to be a valuable alternative to capture dispersion interactions in the G···GLY complexes adequately. On the other hand, AIMD resolves the classical dynamics of the nuclei numerically, and at each time step, the forces are computed to minimize the Kohn-Sham DFT energy functional at a current nuclear configuration. AIMD can allow both equilibrium thermodynamic and dynamical properties of G···GLY interactions at finite temperature to be computed.

The objective is to analyze the adsorption mechanisms of neutral glycine onto graphene oxide models using dispersion-corrected DFT and AIMD approaches and compare their stability when including Stone-Wales structural defects. DFT studies were computed to study the adsorption sites of GLY on G and GO flakes models. A molecular system of C42 atoms (including 16 H atoms saturating dangling bonds) was used to model the graphene flakes. These graphene structures were varied with hydroxyl groups, glycine moieties, and structural defects on the surface. In particular, Stone-Wales (SW) sites

containing 5 and 7 member rings at the center of the graphene flake were used to mimic structural detects. Interactions of GLY neutral molecules with the perfect lattice and SW sites were investigated in both the gas-phase (vacuum) and dissolvent medium (water). AIMD simulations at room-temperature and total relaxation of atomic positions are performed to study adsorption sites on the perfect lattice and SW defects for G and GO models. Interactions of GLY neutral molecules with both models are investigated. DFT and AIMD simulations were carried out using the ORCA quantum chemistry package.

It was found that the GLY molecule interacts with the perfect graphene lattice through noncovalent bonds, and the interaction energy was computed in about −16 kcal/mol. Hydrogen bridges between the hydroxyl groups of GOs models and the $–NH_2$ from GLY lead to total interaction energy of about −24 kcal/mol. However, the –COOH moiety of GLY binds to the hydroxyl groups of GOs with interaction energy of about −33 kcal/mol. The respective interaction energy amounts to about −44.53 kcal/mol for a configuration with Stone-Wales defects. AIMD simulations showed that GLY could stay bonded to the graphene surface to reach a thermodynamic equilibrium (>25 fs) and form simultaneous hydrogen bonds. The molecular dynamics simulations indicate that the complexes and the reservoir tend to thermal equilibrium when the temperature is lowered by about 100 K. The AIMD simulations suggested that after 25 fs, the configuration for the complexes is not different from 0 K.

It was suggested that GLY form mainly noncovalent complexes depending on the G (or GO) model. G and GLY can interact from –16 kcal/mol to -34 kcal/mol. This energy value is about 3 to 9 times the average noncovalent interaction energy. Furthermore, it was shown that Stone-Wales defects cause minor changes in the complex configurations, interaction energies, and thermodynamic stability. AIMD results indicate that after 25 fs, the initial structure at 0 K will not differ after the relaxation of atomic positions at room temperature. In summary, we studied and discussed the interaction mechanisms between

neutral glycine and graphene, graphene oxide models to gain insights into the adsorption interaction, potential energies, and their thermodynamic stability based on DFT and AIMD approaches.

As future work, it is proposed to study the noncovalent interaction for these proposed graphene oxide models with other AAs to gain a complete understanding of the adsorptive properties for these critical biomolecules. It is proposed to increase the time frame for AIMD simulations because biochemical events of interest, such as structural changes in proteins, take place on timescales in the nano or microseconds order. Finally, the basis set level might have an impact on the accuracy of the obtained energies, and thus it is recommendable to extend to a triple-zeta basis set.

1. Introduction

Understanding the fundamentals of the interaction between carbon-based nanomaterials and biomolecules plays a vital role in the development of new nanotechnology and biomedicine devices [1]. This interaction may lead to the formation of biohybrid nanostructures with enhanced physicochemical properties that are governed by the binding properties of the interacting components. In this regard, carbon nanomaterials have been used for detecting biomolecules such as glutathione, where the abnormal concentration can lead to stroke, cancer, and many other degenerative diseases [2]. Furthermore, they have been implemented as part of electrochemical devices to detect enantiomeric d and l amino acids which are important biomarkers because an increase in concentration in urine indicates the presence of renal failure in humans [3].

Carbon has become the most widely used nanomaterial of the 21st century [4] due to its diversified applications. The orbitals of carbon can hybridize into sp, sp^2, and sp^3 configurations, which allows the existence of many allotropes such as amorphous carbon, fullerene, carbon nanowires, graphite, and graphene [5]. Each allotrope has unique chemical, mechanical, thermal, electric, and optical properties [6] which have enabled to development of practical applications in drug delivery, optic devices, electrochemical sensors, tissue engineering, and biosensors [7], [8], [9].

Graphene is the most novel material among these allotropes due to its intrinsic properties such as zero band gap and high conductivity, which facilitates the conduction of electrons, highest mechanical strength, high reactivity to chemical molecules, high specific surface area, and biocompatibility [10], [11]. Graphene is a single monolayer of carbon atoms that consist of sp2 hybridized bonded atoms with a hexagonal honeycomb lattice with a molecular bond length of 1.42 $\dot{A}$. Even though graphene has excellent properties, the use of pristine graphene is challenging due to the synthesis procedure, poor solubility, and agglomeration in

solution [12]. An alternative is to use a top-down method to synthesize graphene with functionalized oxygen groups. Graphene surfaces can be modified by the oxidation methods to functionalize epoxides or hydroxyl groups on the basal plane and carboxylic groups on the edges [13] Graphene oxide (GO) is the result of this process. This enables the tailor of the chemical and physical properties by changing the quantity of hydroxyl, carboxyl, and carbonyl groups to facilitate the specific and selective adsorption of either biological molecules or segments.

Amino acids (AAs) are essential chemical structures in organisms and are known as the building blocks of proteins; AAs can manifest the common physical-chemical properties of biomolecules [14]. Proteins have an important role in biology, so it's of importance the understanding of the interaction between amino acids with nanostructures to obtain a valid first approximation of the mechanism of interaction [15]. Amino acids can be used as biomarkers of diseases; for example, high levels of GLY, CYS, ARG, and TRY are associated with a decrease in the risk of a cardiovascular event. Glycine (GLY, NH_2CH_2COOH) is the simplest of the amino acids and one of the 20 proteinogenic amino acids, these molecules are made of carbon, hydrogen, oxygen, and nitrogen, by evaluating the adsorptive and reactive properties of these amino acids a first approximation can be obtained.

To understand the physical and chemical forces that occur at the bio-organic interface, computational methods based on electronic structure calculations have been developed to gain insights into intermolecular interactions. First principle calculations, Born-Oppenheimer (BO) approximation, and Hartree–Fock (HF) and Density Functional Theory (DFT) methods are used to describe a system as quantum states of many-electron systems [16]. These approaches are based on solving the Schrödinger equation numerically for the system using approximations to reduce the complexity. In the BO approximation is stated that the nucleus is much heavier than the electrons; this neglects the kinetic energy of the nucleus, which results in reducing the Hamiltonian by one term [17]. The HF

method states that the many electrons wave function can be expressed as the product of many one-electron functions [18]. DFT methods use the square of the wave function to determine the information of the system based on the electron probability distribution [19]. These methods allow us to obtain an approximation of the bonding mechanisms, binding energy, charge transfer, and changes in the optical and electronic properties of the interaction. This information facilitates the design of nanodevices for sensing applications with high sensitivity and selectivity.

In recent studies, the interaction between graphene sheets and AAs has been studied; for instance, in the work of Singla et al. [20] the adsorption behavior of Valine, Arginine and aspartic acid on graphene was studied under gas and aqueous phase including Grimme dispersion correction, concluding that the most stable configuration is when the amino acids are parallel to the graphene sheet, the adsorption energy is in the order of the physisorption which offers advantages on the reusability of the graphene sheet. Larijani et al. [21] studied the interaction of graphene with GLY using DFT with a level of theory PBE D3 def2-TZVP. It was demonstrated that glycine can form noncovalent bonds when interacting with graphene with interaction energy of -0.345 eV. Furthermore, water as a solvent was investigated using DFT, the solvent reduces the affinity of the interaction which decreases the interaction energy to -0.251 eV. In other study of Larijani et al. [22] the interaction between perfect and defected graphene and graphene oxide with GLY in gas phase and with water as a solvent was investigated using DFT implementing the Grimme dispersion correction. They demonstrated that GLY can weakly be bound to graphene surface either if it is perfect or with defects with a -0.394 eV and -0.37 eV binding energy respectively which corresponds to a physisorption. Furthermore, with the interaction of graphene oxide they calculated a binding energy of -4.88 eV which can be considered as chemisorption. Finally, the interaction was investigated with water as a solvent, obtaining a binding energy of -0.399 eV which shows a slight

increase in the binding energy in the presence of the solvent. In the work of Rossi et al. [23] the adsorption behavior of GLY on graphene oxide with a hydroxyl group and with a covalent bonded glycine moiety. Where the value of binding energy corresponds to the formation of hydrogen bonds between the epoxy and the amino groups. Furthermore, a high charge transfer is calculated, which is accompanied by an attractive interaction of coulombic nature.

Amino acids have a vital role in living organisms, understanding the interaction with graphene and graphene oxide flakes is of importance to be able to develop new biosensors and nano sensors. The interaction mechanism has been studied as seen in the before mentioned recent works, however the thermodynamic of graphene and graphene oxide interacting with GLY has not been previously studied. The present study provides insightful information to address this fundamental issue by the calculation of physical properties to understand the thermodynamic stability. The results of this work may provide helpful information about the critical aspects of the nature of interaction and on the understating of maintaining the system exergonic to address fundamental issues in the field of nanomaterials and biomedicine.

2. Background

2.1 Carbon nanotechnology

Nanomaterials can be classified by their size and dimensions, there are four types of classification: zero dimensional in which all the three dimensions are in the nanoscale in the range of 1-50 nm such as quantum dots, one dimensional in which one dimension is in the range of 1-100 nm and the other two can be in the macroscale such as nanowires, two dimensional having two dimensions on the nanoscale such as nanosheets and three dimensional where the bulk material is composed of individual blocks in the nanometer scale [24].

Carbon-based nanomaterials are carbon nanostructures that can have different atomic arrangements due to the hybridization states that can be formed when covalent joined to carbon atoms [25]. There are four carbon allotropes that can be created with the different hybridization states: nano diamonds, fullerenes, carbon nanotubes, and graphene. Fullerene was discovered in 1985 by Kroto, is a molecule where 60 carbon atoms are arranged in a soccer ball structure with a sp2 hybridization and is classified as a zero-dimension nanomaterial, it has been used as controlled drug delivery [26]. Carbon nanotubes were discovered in 1991 by lijima, carbon atoms are arranged in cylindrical structure with a sp2 hybridization, and this allotrope has been used as critical elements for the construction of biosensors, strain, and pressure sensor [27].

Graphene was discovered in 2004 by Geim and Novoselov, carbon atoms are arranged in a hexagonal mesh structure where the vertices are the atoms, the main form is in monolayer thus classified as a two-dimensional nanomaterial. Graphene has unique physical properties for example tensile strength of 130.5 GPa [28], zero band gap due to the overlapping of the valance and conduction band in the dirac points [29] and a resistivity in the order of $10^{-6}\Omega$ which is less than that of silver [30]. However, these properties can only be observed experimentally with high lattice order, structural defects knowns as Stone-Wales

defects can be introduced into to the lattice which may modify the physicochemical properties of graphene. They are formed by rotating a C-C bond 90º, which results in the formation of 5-7 ring pair. These defects can be induced by electron beam irradiation [31]. Depending on the distribution and density of the defects new functionalities may be achieved which broaden the applications of graphene [32]. Finally, due to the strain generated in the lattice the potential energy increases, this result in forming a region with higher chemical reactivity.

Graphene can be chemically modified to obtain graphene oxide (GO) by the surface modification (functionalization) with functional groups such as hydroxyl and epoxides groups on the basal plane and carboxylic acids on the edges which results in the transformation of the physicochemical properties of graphene [33]. This functionalization can be either by covalent or noncovalent, in the covalent bond the mechanism involved is the covalent linkage between unsaturated pi-bond carbon and functional groups, is more stable and more robust in terms of binding energy than the noncovalent [34]. Furthermore, the electronic and chemical properties of GO can be tailored easily by the covalent functionalization [35]. In the noncovalent functionalization, the mechanism involved is the pi-pi interaction, ionic interactions, and Van de Waals forces, this method would not cause mayor change in the crystalline structure, but it would cause changes in the electronic distribution [36].

Glycine is one of the proteinogenic amino acids that can be found in nature. GLY the simplest and stable amino acid, it can be found proteins and it is synthesized in the body from serine. GLY in solid-state has three polymorphs at ambient pressure α, β, γ being γ the most stable form [37]. Furthermore, neutral glycine can also be found in the gas phase and in liquid in its zwitterionic phase who arises from the transfer of a proton from the carboxy to the amino groups.

2.2 Density functional theory (DFT)

Quantum mechanics states that the wave function Ψ contains all the information about a system comprising position, momentum, energy, and particle density. For solving Ψ a potential must be $v(r)$ must be specified, place the potential in the Schrödinger equation (SE) an solve for Ψ. This applies for a single body system as well for a many-body system. The Schrödinger equation for a single body system is the following:

$$\left[-\frac{\hbar^2\nabla^2}{2m}+v(r)\right]\Psi(r)=\epsilon\Psi \qquad \text{(Eq. 1)}$$

Where $\hbar$ is the Planck's constant, m is the mass of the particle, $v(r)$ is the potential that characterizes the system, Ψ is the wave function, and ϵ is the energy. For a many-body system, the equation becomes:

$$\left[\sum_i^N\left(-\frac{\hbar^2\nabla^2}{2m}+v(r_i)+\right)+\sum U(r_i,r_j)\right]\Psi(r_1,r_2\ldots r_n)=\epsilon\Psi(r_1,r_2\ldots r_n) \text{ (Eq. 2)}$$

N is the number of electrons in the system and $U(r_i,r_j)$ is the electron-electron interaction, for a coulomb system U can be expressed as:

$$U=\sum_{i<j}U\left(r_i,r_j\right)=\sum_{i<j}\frac{q^2}{|r_i-r_j|} \qquad \text{(Eq. 3)}$$

For the kinetic energy

$$T=-\frac{\hbar^2}{2m}\sum_i\nabla_i^2 \qquad \text{(Eq. 4)}$$

For the potential

$$V=\sum_i v(r_i)=\sum_i\frac{Qq}{|r_i-R|} \qquad \text{(Eq. 5)}$$

where Q is the nuclear charge and R is the nuclear position.

The addition of the electron-electron interactions generates a complex and computationally expensive problem. Even for a system with a few hundred electrons is beyond computational power. The alternative method is to apply DFT

is a quantum mechanical modeling tool which is used to calculate the electronic structure of a many-bodies system approximately. This method has a good balance between computational cost and accuracy for calculating the ground state. DFT transforms a many-body problem into a single-body problem, using the Hohenberg-Kohn (HK) theorem and the Kohn-Sham (KS) equation.

The HK theorem states that the ground states is a functional of the ground-state charge density $n_0(r)$. Ψ contains all the information about the system, hence any ground-state operator is a functional of the ground state density

$$O_0[n_0] = \langle \Psi_0[n_0] | \widehat{O_0} | \Psi_0[n_0] \rangle \qquad \text{(Eq. 6)}$$

Where O_0 is an observable and $\widehat{O_0}$ is an operator with eigenvalue O_0. This equation is known as the 1st HK theorem. Taking into consideration a specific observable, the ground-state energy for a system with potential v can be written as:

$$E_0[n_0] = \left\langle \Psi_0[n_0] \middle| \widehat{H_0} \middle| \Psi_0[n_0] \right\rangle \qquad \text{(Eq. 7)}$$

This demonstrates that to calculate the ground-state energy E_0, the expectation value of the Hamiltonian must be obtained with respect to the ground-state wave function Ψ_0. Furthermore, Ψ_0 must also minimize the energy.

$$E_0[n_0] = \min\left(\left\langle \Psi_0[n_0] \middle| \widehat{H_0} \middle| \Psi_0[n_0] \right\rangle \right) \qquad \text{(Eq. 8)}$$

The operator for energy is the Hamiltonian $\widehat{H_0} = \hat{T} + \hat{U} + \hat{V}$

$$E_0[n_0] = \min\left(\left\langle \Psi_0[n_0] \middle| \hat{T} + \hat{U} + \hat{V} \middle| \Psi_0[n_0] \right\rangle \right) \qquad \text{(Eq. 9)}$$

The kinetic energy T and the electron-electron interaction are independent of the potential of the system V. The potential can be defined with respect to the particle density.

$$E_0[n_0] = \min\left(\left\langle \Psi_0[n_0] \middle| \hat{T} + \hat{U} \middle| \Psi_0[n_0] \right\rangle + \int d^3r \, n(r) v(r) \right) \text{(Eq. 10)}$$

The 2nd HK theorem states that the obtained expectation values of the Hamiltonian with respect to a Ψ other than Ψ_0 will always result in values more significant than the ground state energy. This indicates that when energy is calculated with a density n^*, a value lower than the ground state energy E_0 is not available. Expressed as:

$$E[n_o] \leq E[n^*] \qquad \text{(Eq. 11)}$$

However, the electron-electron interaction remains a problem. By implementing the khon-sham potential is possible to map the many body-problem with an arbitrary U to a single body problem without U. This can be written as

$$E[n] = F[n] + \int d^3r\, n(r)v(r) \qquad \text{(Eq. 12)}$$

where

$$F[n] = T_s[n] + d^3r d^3r' \frac{n(r)n(r')}{|r-r'|} + E_{xc}[n(r)] \qquad \text{(Eq. 13)}$$

$F[n]$ is valid for any potential $v(r)$. The first term is the kinetic energy, the second term is the Hartree potential which describes the electron-electron coulomb repulsion, and the third term represents the variation of the exchange correlation energy. All terms have a solution expect for $E_{xc}[n(r)]$. In Figure 1 a flow chart of the DFT process is seen.

2.3 Exchange correlation functional

The accuracy of the solution for the ground state energy depends on the approximation used in the exchange-correlation functional $E_{xc}[n(r)]$. There are different approximations used to model the exchange-correlation interactions. The local density approximation (LSD) is the simplest and is assumed that the electron density is the same at every position, a more accurate approximation is the generalized gradient approximation (GGA). GGA functional includes not only the density but also the density gradient; with this, the electron density varies

with respect to the position [38] and valuable information can be obtained of how the electron density changes toward a direction.

$$E_{xc}^{GGA}[n(r)] = \int dr\, n(r) f(n(r), \nabla n(r)) \qquad \text{(Eq. 14)}$$

Both functionals have been applied for calculating structural, vibrational, and elastic properties of materials with covalent, metallic and Ionics bonds. There are many functionals that have been implemented using the GGA approximation such as B, CAM, LYP and PBE. All DFT calculations used in this thesis were carried out with the PBE functional.

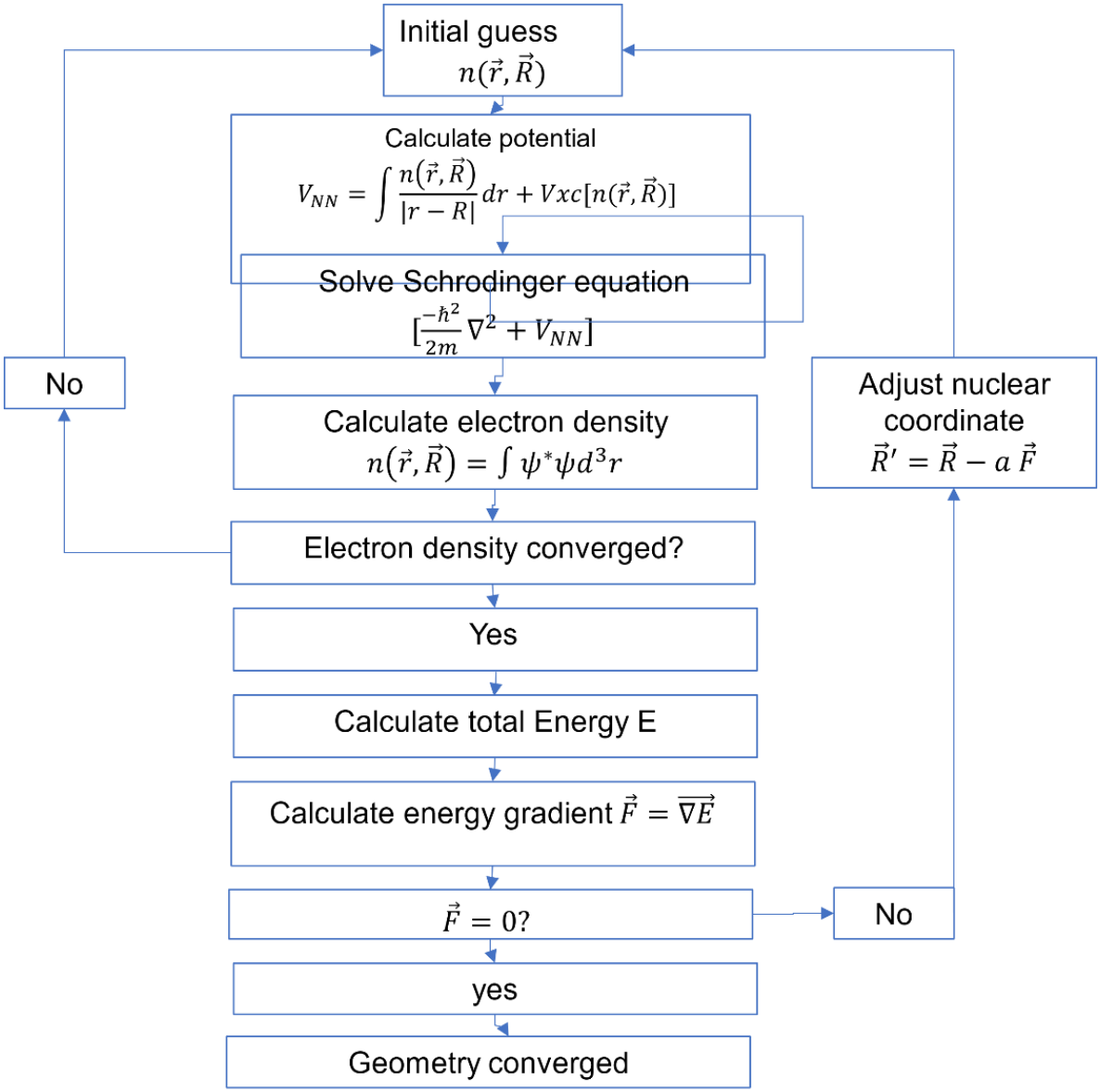

Figure 1. Flow chart of the process that undergoes the DFT calculations for computing the ground state properties and the equilibrium geometries.

2.4 Basis set

The basis set is a computation method for describing the electronic structure of molecules and solids. The wave functions of electrons are described as molecular orbitals, the molecular orbitals are written as an expansion of analytic functions, known as basis set. The basis set are developed and optimized for individual atoms and the basis set for molecules contains the basis set of atoms constituting the molecule. In DFT the basis is used to obtain the density, which determines the energy and all the physical properties [39]. In this thesis the def2-svp basis set is used, where the def2 is a basis set type for the elements from H-Rn which can have different levels from the SV(P) to the QZVPP, these levels are designed to give similar errors across the elements for the given basis set type. The higher the multiple of zeta “triple zeta, quadruple zeta” the more accuracy it can be achieved however the computational power increases.

2.5 Dispersion correction

London dispersion forces are weak intermolecular forces that are responsible for the attractive interactions between nonpolar molecules [40]. They occur when a pair of atoms or molecules are in sufficient proximity and due to temporary dipoles, they induce opposite dipoles in the approaching molecules resulting in a net attractive force [41]. They are a result of long-range electron correlation effects and DFT does not describe this effect. The inclusion of these interactions is indispensable for reaching chemical accuracy and are of importance when aiming for a good description of noncovalent interactions [42]. The energy correction term is the following:

$$E_{Grimme} = E_{DFT} + E_{DFT-D} \qquad \text{(Eq. 15)}$$

where

$$E_{DFT-D} = -\frac{s_6}{2}\sum_{i\neq j}\frac{C_6^{ij}}{R_{ij}^2} f_{damp}(R_{ij}) \qquad \text{(Eq. 16)}$$

Here s_6 is a scaling factor which varies with the functional being used, C_6^{ij} is the dispersion coefficient for each pair of atoms, R_{ij} is the interatomic distance and f_{damp} is a damping function that prevents the divergence of E_{DFT-D} at small R_{ij} values.

2.6 Geometry optimization

Energy minimization is the process of calculating the arrangement in the space of a collection of atoms, where the interatomic force must be close to zero and the position in the potential energy surface (PES) is a stationary point. Energy minimization is used to obtain the structure that corresponds to a particle as it is found in nature, and the geometry of this structure can apply to obtain an approximation for theoretical investigations. Given a set of atoms and a vector containing the positions r, energy can be expressed as a function of position $E(r)$. The objective is to obtain the minimum energy for the system, that is the derivate of the energy with respect to the deposition $\frac{\partial E(r)}{\partial r}$ with this local minimum can be obtained. Furthermore, the second derivate of the energy with respect to the deposition is known as the Hessian matrix $\left(\frac{\partial^2 E}{\partial r_i r_j}\right)_{ij}$ describes the curvature of the PES at a given r.

2.7 Conductor-like Polarizable Continuum Model (CPCM)

To provide insights for nanomedicine and nanobiotechnology applications, the consideration of a solvent is crucial. Human blood contains more than 4,000 components, modeling the interaction with this would require an immense computational power, an approximation of a simpler solvent like water can be used because blood contains between 91%- 92% of water. In the CPCM model, the solvent is treated as polarizable continuum rather than individual molecules interacting with the system [43]. In this method the main parameters are the refractive index and the dielectric constant of the medium.

2.8 Ab initio molecular dynamics (AIMD)

Molecular dynamics (MD) can be used to study the insights of chemical process by solving numerically the classical Newtonian equation of motion for a system with an initial state and set of boundary conditions. MD allows to compute thermodynamic and dynamic properties of a system; the accuracy of the result is dependent on the method by which the force field of the system is specified which are predefined force fields based on empirical data. MD has been applied to approximate to study: liquids, solids, and biological systems, however MD does not include electronic polarization effects and ab initio MD (AIMD) must be implemented to approximate the model correctly. In AIMD, the calculations, temperatures and trajectories are generated by using the forces obtained from the electronic structure which are obtained as the calculations are performed. In this way, electronic variables are not introduced before the calculations and the potential is not assumed to be fixed, which results in obtaining suitable approximated solution of the many-electron problem.

If $R_1, \dots R_N = R$ are the nuclear positions, the AIMD of the nuclei is given by an equation of motion

$$M_I \ddot{R}_I = -\nabla_{\mathrm{I}}[\epsilon_0(R) + V_{NN}(R)], \qquad \text{(Eq. 17)}$$

where ϵ_0 is the ground state energy eigenvalue at the nuclear configuration R and V_{NN} is the nuclear-nuclear coulomb repulsion.

3. Hypothesis and objective

3.1 Hypothesis

The presence of defects and chemical functionalities onto the graphene lattice allows the formation of noncovalent complexes with glycine that can be differentiated by their molecular properties and dynamic stability.

3.2 General objective

Analyze the adsorption mechanisms of neutral glycine onto graphene oxide models using dispersion-corrected DFT and ab-initio molecular dynamics approaches and compare their stability when including Stone-Wales structural defects in both the gas-phase and dissolvent medium.

3.3 Specific objective

- Determine the electronic properties of the noncovalent complexes.
- Calculate the interaction energy between glycine and graphene models.
- Compare the interaction mechanism with and without Stone-Wales defects.
- Compare the interaction mechanism in gas-phase and with dissolvent medium (water).
- Determine thermodynamic stability of the noncovalent complexes.

4. Methodology

The graphene G and graphene oxide GO structures were modeled from a representative graphene flake of $C_{42}H_{16}$. The adsorption site of GLY was studied as occurring onto the -OH moiety for graphene oxide GOH model ($C_{42}H_{18}O$) as well as onto a second glycine chemisorbed graphene oxide GOH-GLY model ($C_{44}H_{23}O_3N$). Representative structures are shown in Figure 1. In the present work, GLY was considered a neutral species. The molecular structures were constructed and visualized using the Avogadro and the SAMSON software.

For the adsorptive process, the adsorption mechanisms were examined in both gas-phase and aqueous environments. On the other hand, the structural defects were introduced into the graphene flakes through Stone-Wales (SW) defects. Theoretically, SW defects can be created in a graphene flake by local rotating a C—C bond by 90° resulting in two pentagons connected by a pair of heptagons, with a possibility of two topologically different orientations. In particular, the SW defect gives rise to 5/7/7/5 defects, which can keep their orientation concerning the graphene axes' rotation due to the graphene flake's symmetry.

Ground-state geometry optimization was carried out using approaches from the density functional theory with dispersion (DFT-D). All DFT-D calculations were performed using the ORCA quantum chemistry software as implemented in the 5.0.1 version. There are others quantum chemistry software such as NWChem, GAUSSIAN, GAMESS, PSI4; however, ORCA is free software that also allows running AIMD calculations. Moreover, ORCA has good built-in basis sets, parallel computing can be used, and the outputs are user friendly.

The optimized structures were computed using a Quasi-Newton method to solve for the local minima of the potential energy surface using three different levels of theory: 1) RKS PBE def2-SVP, 2) RKS PBE D3 def2-SVP, and 3) RKS PBE D3 def2-SVP with CPCM to be able to compare the effects of including the dispersion correction and water as the solvent. The vibrational modes of all the

optimized structures were all positive, which indicates that all structures are stationary points in the geometry optimization. The reported ground-state geometries were obtained with the generalized gradient approximation by Perdew-Burke-Ernzerhof (PBE) functional in conjunction with the Aldrich def2 basis set def2-SVP, which corresponds to a simple-ζ quality basis set with a p-type polarization function added on hydrogen atoms. This basis is used because it is the least complex basis set that includes the polarization function in all the atoms. Furthermore, this basis can be used in almost all atoms. The PBE functional was used because it considers the functional exchange part similarly to the Becke formula and qualitatively accounts for some dispersive interactions. All the electronic structure calculations were studied through DFT using the Grimme D3 dispersion correction method over the PBE functional to account for dispersive interactions between GLY and GO models.

Two series of calculations were tested for the complexes both in a vacuum and in an aqueous medium. The implicit inclusion of medium was conducted via the conductor-like polarizable continuum model (CPCM). The main parameters to define the method are the refractive index and the dielectric constant of the medium (with the value of 80.4 for the dielectric constant of water). CPCM is a continuum solvation model. The solute molecule forms a cavity within the dielectric continuum of permittivity, ε, which represents the solvent. The charge distribution of the solute polarizes the dielectric medium. Thus, the response of the dielectric medium is described by the generation of screening charges on the cavity surface. The screening charges are determined from the boundary condition of vanishing potential on the surface of a conductor. The solvent is described by a continuum that interacts with the charges on the cavity surface, which are in turn determined by the solute, and the problem is solved iteratively.

The relative stability of the GOH···GLY complexes concerning their absolute (Kohn–Sham DFT) energies was performed using the variational supramolecular approach, according to the following standard equation:

$$\Delta E_{ad} = E_{Complex} - (E_{Gs} + E_{GLY})\ (\mathrm{kcal/mol})$$

where, $E_{Complex}$ is the total energy of the complex of an adsorbed amino acid over a graphene model, E_{Gs} is the total energy of the graphene model in its fully optimized geometry, E_{GLY} is the total energy of the glycine in its fully optimized geometry. According to the definition, ΔE_{int}<0 indicates the exergonic nature of the interaction. The electronic properties of the models and from the complex are studied by calculating the HOMO-LUMO energy gap.

Finally, ab-initio molecular dynamics (AIMD) runs were performed using the ORCA MD module to scan the possible conformations of the system at room temperature (298 K). The time step was set at 0.5 fs and run. The run was stopped when an average stable conformation was reached during 25 fs. It was used a canonical ensemble in the NVT approach through the Nosé-Hoover thermostat (NHC). The mass of the hydrogen atom was set to 1. It can be chosen large than one to avoid fluctuations due to the significant time step selected.

5. Results and discussion

5.1 Optimized structures

In the present work, our interest was focused on evaluating the interaction mechanism of GLY with different graphene and graphene oxide models. Six models were used to assess the interaction with GLY. The optimized structures were computed to obtain the most stable energy configuration of each model. As a first approach, the $C_{42}H_{16}$ was used as a graphene model (G) to represent the adsorption site as seen in Figure 2a. This model represents the perfect honeycomb lattice of a graphene flake, which resembles that adopted in a recent adsorption study of amino acids [22]. The graphene oxide (GOH) model includes a hydroxyl group (-OH) that was placed in the basal plane and a hydrogen (H) was also set to obtain a zero net charge as seen in Figure 2b. This GOH model resembles that studied in [23]. The next model consists of graphene oxide with a glycine moiety (GOH-GLY) formed by a covalent bond. The glycine moiety is placed on the edges of the graphene model. This GOH-GLY model was implemented in a recent study [44].

To study the effects of introducing defects on the graphene lattice, in the graphene Stone-Wales model (GSW), the defects are generated by rotating the 90º the central bonded pi carbon atoms which produce heptagons and pentagons as seen in Figure 2d. In the following model (SWGOH) the planar structure is non-conserved as seen in Figure 2e, this is due to the change in the bonding length which increases the strain in the bonds especially at the edges. Finally in the model (SWGOH-GLY), the glycine moiety changes the position to a vertical alignment as seen in Figure 2f, this causes that the structure remains planar which is a more stable energy configuration. The six models were optimized in different levels of theory to be able to compare the introduction of dispersion corrected effects and the effect of water as a solvent, as seen in Supplementary Figures S1 and S2.

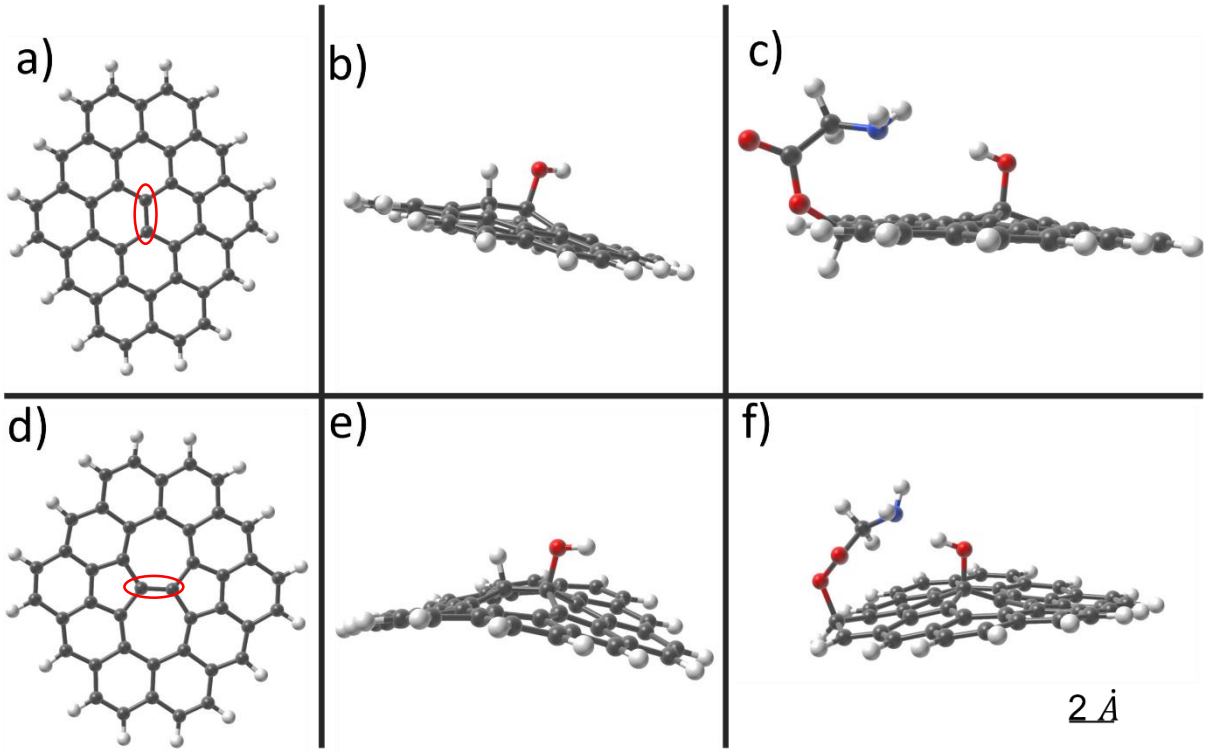

Figure 2. Optimized structures for the graphene flakes as obtained at the RKS PBE-D3/def2-SVP level of theory. Graphene flake, G, (a); Graphene oxide with hydroxyl group, GOH, (b); Graphene oxide with hydroxyl group and covalent glycine, GOH-GLY, (c); Graphene containing Stone-Waals defects, SWG, (d); Graphene oxide with hydroxyl group containing Stone-Waals defects, SWGOH, (e); Graphene oxide with hydroxyl group and covalent glycine containing Stone-Waals defect, SWGOH-GLY, (f).

To study the interaction mechanisms, GLY was placed either on the top or the bottom of each of the models. This interaction can form complexes, as seen in Figure 3. The first step was to calculate the optimized geometries of each complex to obtain the most stable energy configuration. The complex formation of G···GLY as seen in Figure 3a, was only evaluated from the top (T) due to the symmetry of the electron density in G structure. The interaction of glycine on the

GOH model either from the top (T) or the bottom (B) forms the complex GOH·· ·GLY as seen in Figure 3b and in Figure 3c. In Figure 3b, after the optimization process, the amine group from GLY forms a hydrogen bond with the hydroxyl group; furthermore, the parallel orientation of GLY with respect to the graphene oxide sheet and the orientation of the hydrogens from the amine group suggests that this is a stable configuration [21]. The GOH-GLY···GLY complex can be formed when GLY interacts from the top or the bottom, as seen in Figure 3d and in Figure 3e. From Figure 3d the optimized geometry shows that two hydrogen bonds are formed between the carboxylic group of the amine and the hydroxyl group on the basal plane, which demonstrates that the placement of the glycine moiety produces an electron density change which results in the rotation of 180º of the interacting glycine. Finally, from Figure 3c and Figure 3e the interaction from the bottom is shown. The interacting GLY showed two different orientations. Figure 3c shows the hydrogen groups of the amine group are not orientated towards the GOH surface, and thus GLY is not parallel to the surface, whereas in Figure 3e the orientation of GLY is parallel. Even though a hydrogen bond is not formed, noncovalent interaction can take place, suggesting that the formation of the complexes can occur by different mechanisms.

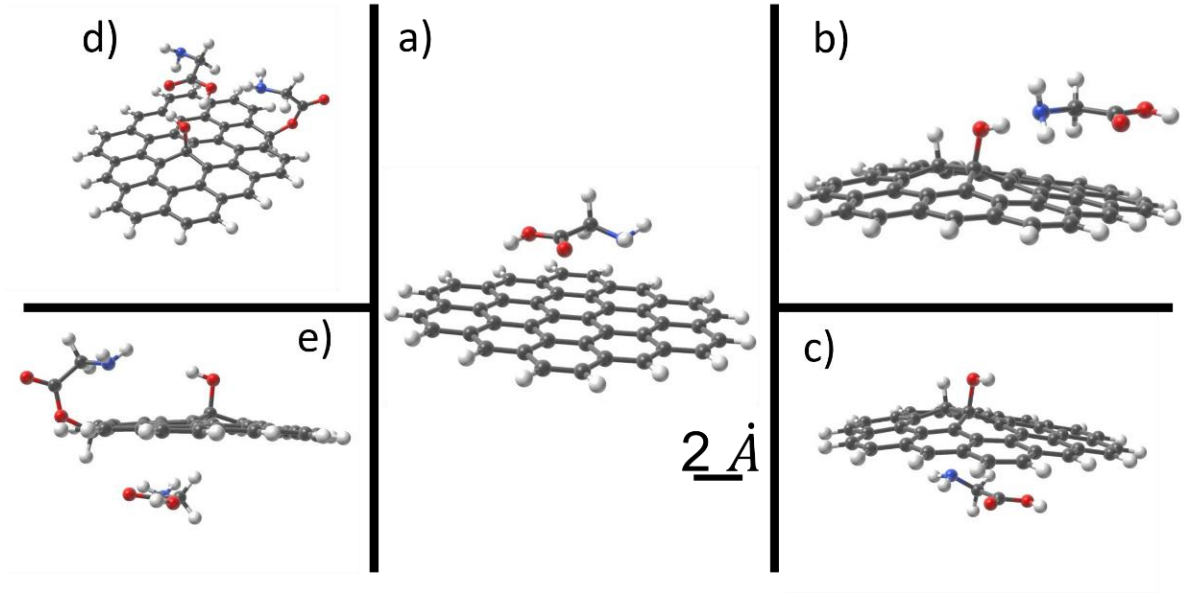

Figure 3. Optimized structures for the noncovalent complexes formed between neutral glycine (GLY) and graphene oxide models as obtained at the RKS PBE-D3/def2-SVP level of theory. GLY interacting with a graphene flake (a); GLY interacting with graphene oxide with hydroxyl group, GOH, from the top (b); GLY interacting with GOH from the bottom (c); GLY interacting with GOH derivatized with a glycine molecule, GOH-GLY, from the top (d); GLY interacting with GOH derivatized with a glycine molecule, GOH-GLY, from the bottom (e).

To study the interaction mechanisms with Stone-Wales defects, GLY was placed either on the top (T) or the bottom (B) of each of the models. This interaction forms complexes, as seen in Figure 4. The first step was to find the optimized geometries of each complex to obtain the most stable energy configuration. The complex formation of SWG···GLY as seen in Figure 4a, was only evaluated from the top due to the symmetry of the electron density in the SWG model. The interaction of GLY in the SWGOH model either from the top or the bottom forms the complex SWGOH···GLY as seen in Figure 4b-c. In Figure 4b, after the optimization process, a convex geometry can be seen, but a hydrogen bond is formed between the amine group and the hydrogen. GLY is at a parallel orientation. When GLY is interacting from the bottom, as seen in Figure 3c a

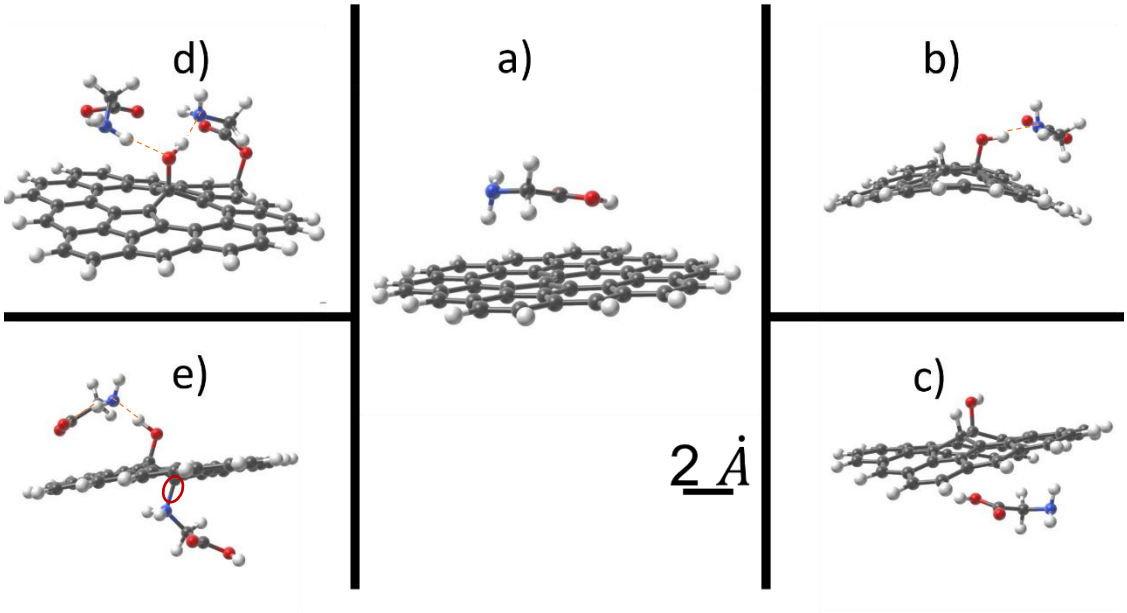

Figure 4. Optimized structures for the noncovalent complexes formed between neutral glycine (GLY) and graphene oxide models containing Stone-Waals (SW) defects as obtained at the RKS PBE-D3/def2-SVP level of theory. GLY interacting with a SW-graphene flake (a); GLY interacting with SW-graphene oxide with hydroxyl group, SWGOH, from the top (b); GLY interacting with SWGOH from the bottom (c); GLY interacting with SWGOH derivatized with a glycine molecule, SWGOH-GLY, from the top (d); GLY interacting with SWGOH derivatized with a glycine molecule, SWGOH-GLY, from the bottom (e).

parallel orientation was obtained and the carboxylic group from GLY is closer than the amine to the GOH surface. The SWGOH-GLY···GLY complex interacts with GLY from the top or the bottom, as seen in Figure 4d-e. When GLY interacts from the top, as seen in Figure 4d, two hydrogen bonds are formed between the amine groups of each GLY. When GLY interacts from the bottom, as seen in Figure 4e, the covalent bond from the GLY moiety is broken; this results in the formation of a hydrogen bond, and the interacting glycine from the bottom forms a covalent bond between the nitrogen and the carbon.

By comparing the optimized geometries, SW defects induce an influence in the final geometries. For the G and SWG models, the final structure has not a significant change caused by the introduction of the defects. However, for the

GOH and SWGOH models, curvature and a sinusoidal shape are obtained, which agrees with past studies that demonstrate that the defects cause ribbon-like structures or sine/cosine shapes [45], [46]. Finally, for the GOH-GLY and SWGOH-GLY models, the effect of the defects is more visible due to in the optimized structure a covalent bond is formed. In all the models, a noncovalent interaction can be seen, except for the SWGOH-GLY with the glycine interacting from the bottom.

5.2 Electronic properties

In molecular interactions, the molecular orbitals are of interest. The difference in energy from the HOMO-LUMO results in the energy gap, a molecule with a high energy gap has kinetic stability and low chemical reactivity [47]. The energy gap allows to determine the charge transfer interaction, the electronic and optical properties of the molecules. In Table 1 the calculated values for the HOMO-LUMO energy gap of the six models is reported in gas phase and in water. The minimum energy gap of 0.1356 eV is achieved with the SWGOH-GLY model and the higher energy gap of 2.0483 eV is achieved with the SWGOH model, the other models are between these range of values. When the systems are simulated in the water a change in the energy gap between .002 to .05 eV was obtained. These results demonstrates that the introduction of structural defects has a significant impact on the optical properties of graphene, these changes in the energy gap are due to the perturbation of the energy state near the Dirac cone which results in the opening or closing of the energy gap [48].

Table 1. HOMO-LUMO energy gap (in eV) calculated at the PBE/SVP, with dispersion-correction (D3) and dissolvent effect (CPCM) for the graphene flake, G; Graphene oxide with hydroxyl group, GOH; Graphene oxide with hydroxyl group and covalent glycine, GOH-GLY; Graphene containing Stone-Wales defects, SWG; Graphene oxide with hydroxyl group containing Stone-Wales defects, SWGOH; Graphene oxide with hydroxyl group and covalent glycine containing Stone-Wales defect, SWGOH-GLY.

Systems	PBE/SVP (gas-phase)	PBE-D3/SVP (gas-phase)	PBE-D3/SVP (water)
G	1.6025	1.6040	1.6078
GOH	1.0594	1.0598	1.0585
GOH-GLY	1.5099	1.5053	1.5068
SWG	1.4143	1.4182	1.3627
SWGOH	2.0474	2.0483	2.0644
SWGOH-GLY	0.1354	0.1356	0.1868

Upon the interaction of GLY with the different models, the HOMO-LUMO gap energies of each model changes as seen in Table 2. This increase or decrease in the gap energies is due to the complex formation which causes that the electron density from the HOMO of GLY transfers to the LUMO of the models. This result agrees with the model presented in [49]. In these calculated values, the SWGOH-GLY···GLY (T) complex has the minimum gap energy of 0.1236 eV and the SWGOH···GLY (B) model has the maximum gap energy of 2.0289 eV when the model is evaluated at the gas phase. When the models are simulated in water, the same trend is obtained. However, the model SWGOH-GLY···GLY (B) has an increase in the gap energy of 1.1262 eV.

Table 2. HOMO-LUMO gap energies (in eV) calculated at the PBE/SVP, with dispersion-correction (D3) and dissolvent effect (CPCM) for the noncovalent complexes GLY interacting with a graphene flake; GLY interacting with graphene oxide with hydroxyl group, GOH, from the top (T); GLY interacting with GOH from the bottom (B); GLY interacting with GOH derivatized with a glycine molecule, GOH-GLY, from the top (T); GLY interacting with GOH derivatized with a glycine molecule, GOH-GLY, from the bottom (B). For comparison these gap energies are showed for the complexes containing Stone-Wales defects.

Complexes	PBE/SVP (gas-phase)	PBE-D3/SVP (gas-phase)	PBE-D3/SVP (water)
G···GLY (T)	1.6051	1.6051	1.6085
GOH···GLY (T)	1.3161	1.0760	1.0587
GOH···GLY (B)	1.0745	1.0994	1.0653
GOH-GLY···GLY (T)	1.4851	1.4205	1.3890
GOH-GLY···GLY (B)	1.4450	1.4107	1.4681
SWG···GLY (T)	1.4072	1.4095	1.3610
SWGOH···GLY (T)	2.0225	2.0087	2.0443
SWGOH···GLY (B)	1.9950	2.0289	2.0566
SWGOH-GLY···GLY (T)	0.1701	0.1236	0.1933
SWGOH-GLY···GLY (B)	0.1189	0.3899	1.5161

5.3 Interaction energy

The interaction energies of the complexes are seen in Table 3, the lowest energy was calculated for the G···GLY (T) complex with interaction energy of -16.32 kcal/mol and the highest energy for the GOH-GLY···GLY (T) complex with interaction energy of -33.29 kcal/mol. The interaction energy for the G···GLY (T) complex is 2 times higher than previously reported values in a similar model [22], this result suggests that the glycine molecule is physisorbed to the surface. Furthermore, in the model GOH···GLY (T) the interaction energy is also 2 times higher than previously reported values in the same model [23], this confirms that an overestimation was made in our calculation due to the implementation of the simplest basis set. Furthermore, this increase in interaction energy is due to the formation of one hydrogen bond between the nitrogen from the amine group and the hydrogen of the hydroxyl group. In the model GOH-GLY····GLY (T), the

increase in the interaction energy is due to the formation of two hydrogen bonds with the carboxylic group which has a higher electronegativity. When solvent is introduced into the system, a decrease in the interaction energies is obtained. This is because water reduces the affinity of glycine towards our graphene models due to the existence of polar bonds in the structure of the glycine [21].

To evaluate the interaction of glycine with the models containing SW defects, the interaction energies were calculated. In Table 4, the obtained values of the interaction energies for the complexes are seen. The model with the lowest energy is SWG···GLY (T) with a value of -16.92 kcal/mol and highest energy for the SWGOH-GLY···GLY (B) with a value of -44.53 kcal/mol. The interaction energy for the SWG···GLY (T) complex is 2 time higher that previously reported values in a similar model [22]. The value obtained for the SWGOH-GLY···GLY (B) is in the order of the covalent bond which is confirmed in Figure 3e. A similar trend on the decrease of the interaction energies when solvent is introduced is seen, however an increase in the interaction energy of the model SWGOH-GLY···GLY (B) is seen which could be associated to the decrease in affinity of the top glycine, which enables the system to configurate into a more stable energy configuration.

Table 3 Interaction energies (in kcal/mol) as calculated at the PBE/SVP, with dispersion-correction (D3) and dissolvent effect (CPCM) for the noncovalent complexes between GLY neutral interacting with a graphene flake; GLY interacting with graphene oxide with hydroxyl group, GOH, from the top (T); GLY interacting with GOH from the bottom (B); GLY interacting with GOH derivatized with a glycine molecule, GOH-GLY, from the top (T); GLY interacting with GOH derivatized with a glycine molecule, GOH-GLY, from the bottom (B).

Complexes	PBE/SVP (gas-phase)	PBE-D3/SVP (gas-phase)	PBE-D3/SVP (water)
G···GLY (T)	-6.93	-16.32	-13.54
GOH···GLY (T)	-17.79	-24.50	-12.69
GOH···GLY (B)	-10.75	-20.40	-13.04
GOH-GLY···GLY (T)	-24.82	-33.29	-20.42
GOH-GLY···GLY (B)	-9.34	-18.33	-15.41

Table 4. Interaction energies (in kcal/mol) as calculated at the PBE/SVP, with dispersion-correction (D3) and dissolvent effect (CPCM) for the noncovalent complexes containing Stone-Wales (SW) defects. GLY interacting with a SW-graphene flake at the top (T); GLY interacting with SW-graphene oxide with hydroxyl group, SWGOH, from the top (T); GLY interacting with SWGOH from the bottom (B); GLY interacting with SWGOH derivatized with a glycine molecule, SWGOH-GLY, from the top (T); GLY interacting with SWGOH derivatized with a glycine molecule, SWGOH-GLY, from the bottom (B).

Complexes	PBE/SVP (gas-phase)	PBE-D3/SVP (gas-phase)	PBE-D3/SVP (water)
SWG···GLY (T)	-7.10	-16.92	-11.74
SWGOH···GLY (T)	-16.29	-22.60	-19.55
SWGOH···GLY (B)	-9.12	-19.08	-12.64
SWGOH-GLY···GLY (T)	-18.21	-19.71	-14.16
SWGOH-GLY···GLY (B)	-6.95	-44.53	-62.77

5.4 Thermodynamic stability

DFT studies are computed in a vacuum environment, the molecules are in gas-phase and the temperature of the system is 0 K. To gain insights on how the system is transformed when time and temperature is involved AIMD calculations are performed to evaluate the thermodynamic stability of the complexes. AIMD combines the results from the DFT with thermodynamic variables and statistical mechanics. In Figure 5, the results for the AIMD of the G···GLY and SWG···GLY complexes are shown, in these results the potential energy represents the Helmholtz free energy. This energy is the maximum amount of work that a system can perform in a thermodynamic process. In Figure 5a the G···GLY (T) and SWG···GLY (T) complexes are shown in gas-phase, after 8 fs the complexes reach the highest potential energy, which is between 160 and 150 kJ/mol and the temperature reaches the minimum of 150 K and 160 K. This decrease in temperature and increase in energy is in agree with the first law of thermodynamics, temperature is being transfer to the complex which results in an

increase in the potential energy of the complex. This increase in energy allows the complex to change the atomic arrangement, which results in a new configuration of the system. Then after 9 fs the system starts to relax into a more stable energy configuration and proceeds to transfer energy to the environment which leads to an increase in the temperature, this trend where the complex transfers between 40 kJ/mol and 60 kJ/mol continues until reaching 25 fs. By reaching this time frame, thermodynamic stability is achieved because the complex has less energy to be able to form a new configuration. When SW defects are introduced in the lattice, less endothermic process is seen in the first 8 fs, which means that defects enhance the ability of forming more stable configurations. After 9 fs a similar trend in G model is observed. When solvent is introduced into the system, as seen in Figure 4b, a similar trend can be seen of reaching thermodynamic stability after 25 fs. However, the solvent enables the SW defect model to gain more potential energy. The results obtained from the AIMD analysis agree with the results obtained from the geometry optimization in gas-phase where GLY interacts in the same orientation with G or SW, which suggests that the introduction of defects in graphene has no significant effect on enhancing the stability in this model. Furthermore, the interaction energies are close in value with a difference of 0.6 kcal/mol which could explain the same behavior of the fluctuations of the energies. Regarding the model interacting with the solvent, there is a difference of 1.8 kcal/mol in the interaction energies from the complexes. This should make the behavior of the fluctuations in energy behave differently; however, due to the solvent effects, the energies in each endothermic peak are similar.

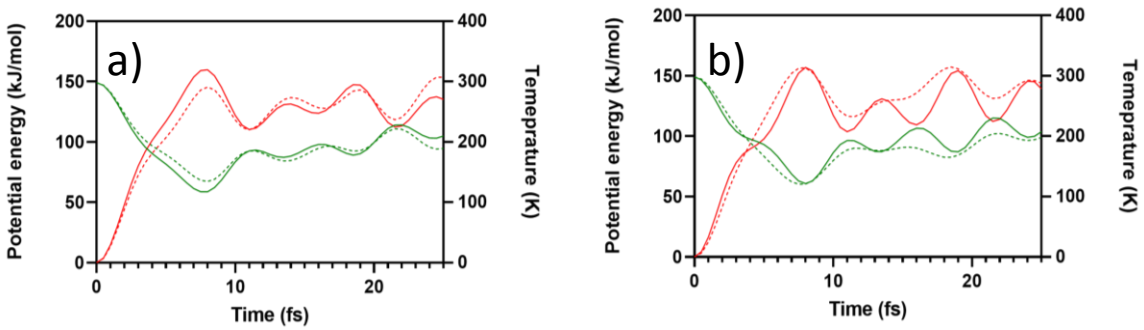

Figure 5. Ab-initio molecular dynamics (AIMD) simulations to scan the possible conformations for interactions between graphene and glycine at room temperature (298 K). The time step was set at 0.5 fs. Solid lines correspond to G-GLY(T) in perfect lattice in, while dashed lines represent SWG-GLY(T) graphene flakes. Potential energies (in kJ/mol) are in red; temperatures (in K) are in green color. a) gas-phase, b) solvent.

The AIMD results for the GOH and SWGOH complexes interacting from the top or the bottom are shown in Figure 6. In Figure 6a and Figure 6c, the interaction of GOH···GLY from the top and from the bottom in the gas-phase is shown. From these results, the complex GOH···GLY (T) goes through an endothermic process where the potential energy is raised to a maximum of 150 kJ/mol then the potential energy fluctuates between 140 kJ/mol and 150 kJ/mol. The maximum potential energy of the complex GOH···GLY (B) is 165 kJ/mol then a downtrend with an energy fluctuation between 130 kJ/mol and 140 kJ/mol. The GOH···GLY (T) complex can absorb less energy which indicates that the complex is more thermodynamic stable than the GOH···GLY (B) complex; this could be explained by the hydrogen bond formed between the two systems. From the SWGOH models the AIMD results show similar behavior to the models not containing defects, in these models, the effect of the SW defects does not have an important influence in the thermodynamic stability of the system. Comparing the models in their solvent interaction as seen in Figure 6b and 6d, the solvent has a

significant influence on the transition energies that can be formed in the model GOH···GLY (T) and in the initial energy that the complex can absorb, for the model GOH···GLY (B) a similar trend can be seen when the complex is in gas phase. For the SW defects in these models the energy difference that the complexes can absorb and the trend in which the complexes release the energy resembles the models not containing defects. In SW defects the solvent has not a significant influence in the potential energy.

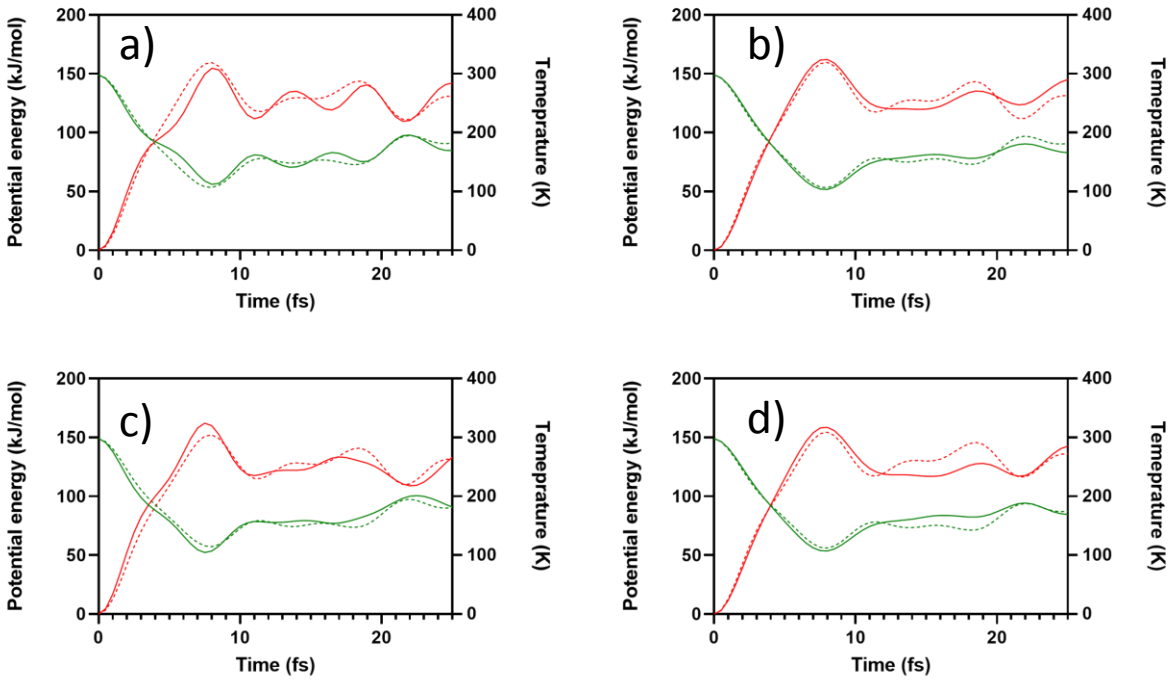

Figure 6. Ab-initio molecular dynamics (AIMD) simulations to scan the potential energies for the complexes formed between GOH and GLY at room temperature (298 K). The interaction can occur either when GLY interacts form the top of the GOH flake, or from the bottom. Solid lines correspond to a lattice perfect GOH, while dashed lines represent to SWGOH flakes. Potential energies (in kJ/mol) are in red; temperatures (in K) are in green colors. The time step was set at 0.5 fs up to 25 fs. a) gas-phase of GOH ···GLY (T), b) solvent interaction of GOH ···GLY (T), c) gas-phase of GOH ···GLY (B), d) solvent interaction of GOH ···GLY (B).

In Figure 7, the AIMD results for the complex of GOH-GLY & SWGOH-GLY interacting from the top or the bottom are shown. In Figure 7a and Figure 7c, the interaction of GOH-GLY···GLY from the top or from the bottom in gas phase is shown. The complex GOH-GLY···GLY (T) goes through an endothermic process where the potential energy is raised to a maximum of 190 kJ/mol then the potential energy fluctuates between 140 kJ/mol and 150 kJ/mol. In comparison with the SWGOH-GLY···GLY (T) complex, a maximum of the potential energy of 165 kJ/mol is calculated then the potential energy fluctuates between 130 kJ/mol and 160 kJ/mol. The GOH-GLY···GLY (T) complex has interaction energy of -33.29 kcal/mol and the SWGOH-GLY···GLY (T) complex -19.71 kcal/mol. This demonstrates that the potential energy of the complex can be higher even for a model with more interaction energy. The following complex GOH-GLY···GLY (B) reaches a maximum of 155 kJ/mol then the potential energy fluctuates between 140 kJ/mol and 160 kJ/mol. In comparison with the SWGOH-GLY···GLY (B) complex reaches a maximum of 180 kJ/mol then the potential energy fluctuates between 130 kJ/mol and 160 kJ/mol. This increase in potential energy of the SW model could be attributed to the non-covalent bonded glycine on the top, which during the endothermic process is freer to move. In Figure 7b and Figure 7d, the interaction of GOH-GLY···GLY from the top or from the bottom in solvent interaction is shown. In both models, a decrease in the fluctuations of the potential energy is seen, and a similar trend onto thermodynamic stability.

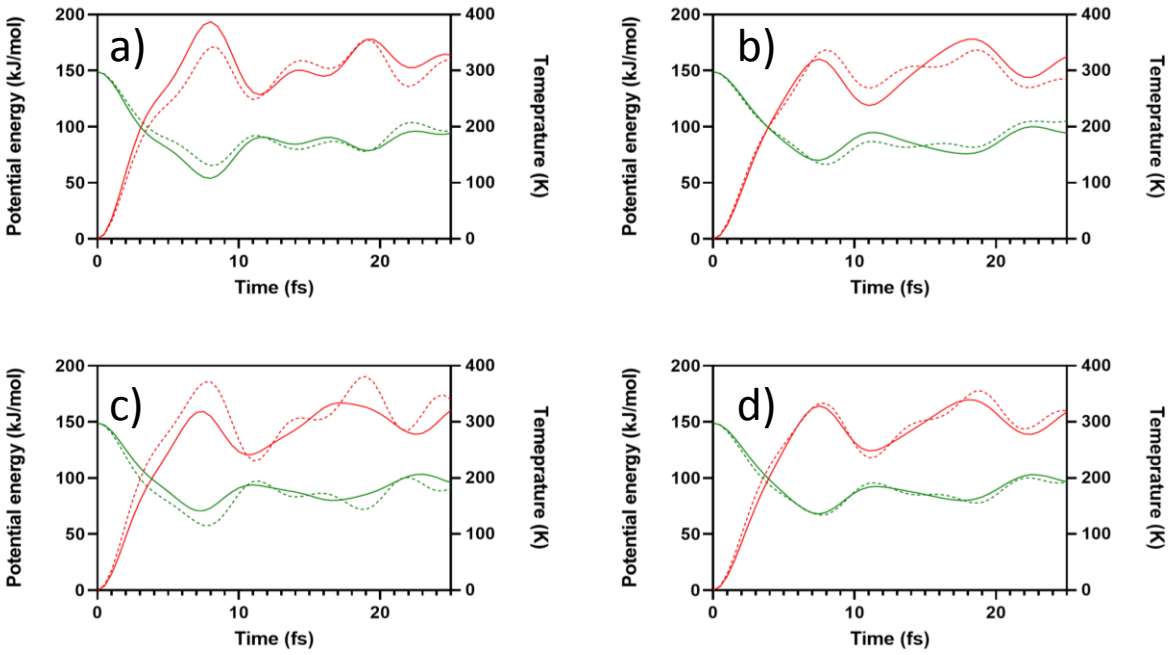

Figure 7. Ab-initio molecular dynamics (AIMD) simulations to scan the potential energies for the complexes formed between GOH-GLY and GLY at room temperature (298 K). The interaction can occur either when GLY interacts form the top of the GOH-GLY flake, or from the bottom. Solid lines correspond to a lattice perfect GOH-GLY, while dashed lines represent to SWGOH-GLY flakes. Potential energies (in kJ/mol) are in red; temperatures (in K) are in green colors. The time step was set a at 0.5 fs up to 25 fs. a) gas-phase of GOH-GLY ···GLY (T), b) solvent interaction of GOH-GLY ···GLY (T), c) gas-phase of GOH-GLY ···GLY (B), b) solvent interaction of GOH-GLY ···GLY (B).

5.5 Comparison with other models

The interaction energies for our proposed model are compared with the models of Larijani and Rossi, as seen in Table 5. For the G/SWG···GLY in gas-phase model a difference of 7.64 kcal/mol and 7.74 kcal/mol, this could be attributed to Larijani using a higher basis set which suggests that our results are overestimated or that our models have formed a more stable complex. The values for the solvent in Larijani indicates an increase in the interaction energy

and in the results of this work the interaction energy decrease. This demonstrates that model implemented by Larijani get binder tighter when the solvent is present and in our model the solvent has the effect of decreasing the interaction energy. For the model GOH···GLY (T) when the system is interacting with water, a difference from Rossi model of 2.54 kcal/mol is observed. In their DFT model a TZVP basis was used; however, our interaction energies are not that different. This suggests that the solvent has a significant substantial effect on the interaction energies.

Table 5. Comparison for the interaction energies (kcal/mol)

Complexes	This work	Larijani [22], [21]	Rossi [23]
G···GLY (T)	-16.32	-8.99	X
gas-phase (water)	(-13.54)	(-9.20)	(X)
GOH···GLY (T)	-24.50	X	X
gas-phase (water)	(-14.16)	(X)	(-11.62)
SWG····GLY (T)	-16.29	-8.53	X
gas-phase (water)	(-11.74)	(X)	(X)
SWGOH···GLY (T)	-19.71	X	X
gas-phase (water)	(-14.16)	(X)	(X)

6. Conclusion

In conclusion, the interaction mechanism of glycine with different graphene/graphene oxide models was investigated through computational methods to gain an insight into the interaction process. Ab initio molecular dynamics and density functional theory methods were used to investigate the adsorptive nature of glycine and to calculate the physical properties of these phenomena, such as potential energies, interaction energies, gap energies, and thermodynamic stability. Even though large biomolecules are more complex than the glycine studied in this thesis, they all include carboxylic groups, amine, and hydroxyl groups which can serve as active sites. Hence the results from this work could be extrapolated to understand the interaction mechanisms of more complex biomolecules. Following the objectives of this study, the interaction mechanisms of glycine were studied under six different models where defects are introduced and with three different levels of theory. The results from the interaction energies demonstrated that all the complexes formed a non-covalent interaction except for a model containing defects that formed a covalent bond. The obtained values are in the range of –16 kcal/mol to -34 kcal/mol. However, these energies values are about 3 to 9 times the average non-covalent interaction energy. Furthermore, the gap energies demonstrated that the complexes can be semiconductors with different gap energies, which are in the 0.3 to 2.5 eV. Furthermore, the most stable configurations of the models agree with past studies. Finally, the AIMD calculation demonstrated that all the complexes are thermodynamically stable in a 25-fs period.

7. Outlook

In future work, the increase of the basis set should be implemented to increase the accuracy of our results. An increase to a QTZVP set should confirm the reliability of the results presented in this thesis and will allow us to determine the effect of implementing a higher basis. Furthermore, AIMD calculations in a window time of the nanoseconds which is the typical time for a reaction to occur. In this thesis, due to the time shortage, studies could not be carried out in this time frame. However, it is of importance to understand the effect that this will have on our results. Furthermore, our results suggest that these models could be integrated into sensing platform's devices due to the energy band and the interaction energies obtained. To be able to integrate any of the models studied to a device, selectivity and sensitivity should be tested to detect specific biomolecules of interest, such as cardio biomarkers. Another application that this model could have is to be implemented as a coating agent for enhancing solar applications. As reported in this thesis, the energy gap of graphene was easily modified by the introduction of hydroxyl groups and covalently bonded glycine to obtain an energies gap between 1 and 1.5 or by the introduction of defects. By these modifications on the energy gap of the graphene, it could be used to coat materials to have a better performance under UV radiation.

8. Bibliography

[1] C. Sanchez, K. J. Shea and S. Kitagawa, "Recent progress in hybrid materials science," *chemical society reviews,* vol. 40, no. 2, p. 471, 2011.

[2] S. Wua, X. Lana, F. Huanga, Z. Luoc, H. Jub and C. Menga, "Selective electrochemical detection of cysteine in complex serum by graphene nanoribbon," *biosensors and bioelectronics,* vol. 32, pp. 293-296, 2012.

[3] A. Martín, P. Batalla, J. Hernández-Ferrer, M. T. Martínez and A. Escarpa, "Graphene oxide nanoribbon-based sensors for the simultaneous bio-electrochemical enantiomeric resolution and analysis of amino acid biomarkers," *Biosensors and Bioelectronics,* vol. 68, pp. 163-167, 2015.

[4] H. HAick, Nanotechnology and Nanosensors Introduction to Nanotechnology., Technion Israel Institute of technology, 2013.

[5] R. Rauti, M. Musto, S. Bosi, M. Prato and L. Ballerini, "Properties and behavior of carbon nanomaterials when interfacing neuronal cells: how far have we come?," *Carbon,* vol. 143, no. 2019, p. 430, 2018.

[6] S. A. MohdZobir, S. AbdulRashid: and TonglingTan, "Recent Development on the Synthesis Techniques and Properties of Graphene Derivatives," in *Synthesis, Technology and Applications of Carbon Nanomaterials*, Elsevier, 2019, p. 77.

[7] P.Viswanathan and R.Ramaraj, "Functionalized Graphene Nanocomposites for Electrochemical Sensors," in *Graphene-Based Electrochemical Sensors for Biomolecules*, Elsevier, 2019, p. 43.

[8] D. Maiti, X. Tong, X. Mou and K. Yang, "Carbon-Based Nanomaterials for Biomedical Applications: A Recent Study," *Frontiers in pharmacology,* vol. 9, p. 1401, 2019.

[9] M. E. Ayhan, "A single-step fabrication of Ag nanoparticles and CVD graphene hybrid nanostructure as SERS substrate," *Microelectronic Engineering,* vol. 233, p. 111421, 2020.

[10] G. Yildiz, M. Bolton-Warberg and F. Awaja, "Graphene and graphene oxide for bio-sensing: General properties and the effects of graphene ripples," *Acta biomaterialia,* vol. 131, no. 1, pp. 62-79, 2021.

[11] K. Bolotin, K. Sikes, Z. Jiang, M. Klima, G. Fudenberg, J. Hone, P. Kim and H. Stormer, "Ultrahigh electron mobility in suspended graphene," *Solid state communication,* vol. 149, no. 9, pp. 351-355, 2008.

[12] A. T. Smith, A. M. LaChance, S. Zeng, B. Liu and L. Sun, "Synthesis, properties, and applications of graphene oxide/reduced graphene oxide and their nanocomposites," *Nano Materials Science,* vol. 1, no. 1, pp. 31-47, 2019.

[13] I. A. Vacchi, J. Raya, A. Bianco and C. Ménard-Moyon, "Controlled derivatization of hydroxyl groups of graphene oxide in mild conditions," *2D materials,* vol. 5, no. 3, 2018.

[14] K. Gao, G. Chen and D. Wub, "A DFT study on the interaction between glycine molecules/radicals and the (8, 0) SiCNT†," *Physical Chemistry Chemical Physics,* vol. 16, pp. 17988-17997, 2014.

[15] O. D. Sparkman, Z. E. Penton and F. G. Kitson, "Amino Acids," in *Gas Chromatography and Mass Spectrometry (Second edition)*, Elsevier, 2011, p. 265.

[16] K. H.Hopmann and F. Himo, "Quantum Chemical Modeling of Enzymatic Reactions – Applications to Epoxide-Transforming Enzymes," in *Comprehensive Natural Products II*, Elsevier, 2010, p. 719.

[17] M. Born and R. Oppenheimer, "Zur Quantentheorie der Molekeln," *Annalen der Physik,* vol. 389, p. 457, 1927.

[18] V. Fock, "Naherungsmethode zur Losung des quantenmechanischen Mehrkorperproblems," *Zeitschrift für Physik,* vol. 61, pp. 126-148, 1930.

[19] I. M. Sharafeldin, J. E. Fitzgerald, H. Fenniri and N. K. Allam, "Computational Modeling for Biomimetic Sensors," in *Biomimetic Sensing Volume* , New york, NY, Springer, 2019, pp. 195-210.

[20] P. Singla, M. Riyaz, S. Singhal and N. Goel, "Theoretical study of adsorption of amino acids on graphene and BN sheet in gas and aqueous phase including empirical DFT Dispersion correction," *Physical Chemistry Chemical Physics,* vol. 18, pp. 5597-5604, 2016.

[21] H. T. Larijani, M. Jahanshahi, M. D. Ganji and M. H. Kiani, "Computational studies on the interactions of glycine amino acid with graphene, h-BN and h-SiC monolayers," *Physical Chemistry Chemical Physics,* vol. 19, p. 1896, 2017.

[22] H. T. Larijani, M. D. Ganji and M. Jahanshahi, "Trends of amino acid adsorption onto graphene and graphene oxide surfaces: a dispersion corrected DFT study," *The Royal Society of Chemistry,* vol. 5, no. 113, pp. 92843-92857, 2015.

[23] A. C. Rossi-Fernández, N. Villegas-Escobar, D. Guzmán-Angel and S. Gutiérrez-Oliva, "Theoretical study of glycine amino acid adsorption on graphene oxide," *Journal of Molecular Modeling,* pp. 26-33, 2020.

[24] B. Malhotra and A. Ali, Nanomaterials for Biosensors, Elsevier, 2017.

[25] R. Rauti, M. Musto, S. Bosi, M. Prato and L. Ballerini, "Properties and behavior of carbon nanomaterials when interfacing neuronal cells how far have we come?," *Carbon,* vol. 18, p. 31049, 2018.

[26] G. M. Raghavendra, K. Varaprasad and T. Jayaramudu, "Chapter 2 - Biomaterials: Design, Development and Biomedical Applications," in *Nanotechnology Applications for Tissue Engineering*, William Andrew, 2015, pp. 21-44.

[27] M. Zhou, Z. Wang and X. Wang, "Carbon Nanotubes for Sensing Applications," in *Industrial Applications of Carbon Nanotubes*, Elsevier, 2017, pp. 129-150.

[28] C. Lee, X. Wei, J. Kysar and J. Hone, "Measurement of the elastic properties and intrinsic strength of monolayer graphene," *Science,* vol. 321, pp. 385-388, 2008.

[29] R. Zan, Q. Ramasse, U. Bangert and K. Novoselov, " Graphene reknits its holes," *Nano letters,* vol. 12, p. 3936, 2012.

[30] C. R. Holkar, S. S. Jain, A. J. Jadhav and D. V. Pinjari, "SCALE-UP TECHNOLOGIES FOR ADVANCED NANOMATERIALS FOR GREEN ENERGY: FEASIBILITIES AND CHALLENGES," *Nanomaterials for Green Energy,* pp. 433-455, 2018.

[31] A. W. Robertson, C. S. Allen, Y. A. Wu, K. He, J. Olivier, J. Neethling, A. I. Kirkland and J. H. Warner, "Spatial control of defect creation in graphene at the nanoscale," *Nature communications,* vol. 3, p. 1144, 2012.

[32] TaoXu and LitaoSun, "Structural defects in graphene," in *Defects in Advanced Electronic Materials and Novel Low Dimensional Structures*, Elsevier, 2018, p. 137.

[33] I. Khosravi, Z. Shahryari, S. M. J. Moghadas, H. T. Sarraf and M. Yeganeh, "The application of graphene oxide as corrosion barrier," in *Corrosion Protection at the Nanoscale*, Elsevier, 2020, pp. 127-140.

[34] Y. J. Lau, F. S. A. Khan, N. Mubarak, S. Y. Lau, H. B. Chua, M. Khalid and E. Abdullah, "Functionalized carbon nanomaterials for wastewater treatment," in *Industrial Applications of Nanomaterials*, Elsevier, 2019, pp. 283-311.

[35] G. V, T. JN, K. KC, P. JA, B. AB, K. KS and Z. R, "Noncovalent Functionalization of Graphene and Graphene Oxide for Energy Materials, Biosensing, Catalytic, and Biomedical Applications," *Chem Rev.,* vol. 9, no. 116, p. 5464, 2016.

[36] V. Georgakilas, M. Otyepka, A. B. Bourlinos, V. Chandra, N. Kim, K. C. Kemp, P. Hobza, R. Zboril and K. S. Kim, "Functionalization of Graphene: Covalent and Non-Covalent Approaches, Derivatives and Applications," *Chem rev,* no. 112, p. 6156, 2012.

[37] G. L. Perlovich, L. K. Hansen and A. Bauer-Brandl, "The Polymorphism of Glycine. Thermochemical and structural aspects," *Journal of Thermal Analysis and Calorimetry volume ,* vol. 66, pp. 699-715, 2001.

[38] K. A. Baseden and J. W. Tye, "Introduction to Density Functional Theory: Calculations by Hand on the Helium Atom," *J. Chem. Educ.,* vol. 91, p. 2116, 2014.

[39] E. Perlt, Basis Sets in Computational Chemistry, Springer, Cham, 2021.

[40] R. M. R. Sanghvi and H. (. Zhu, "Solubility of Pharmaceutical Solids," in *Developing Solid Oral Dosage Forms (Second Edition)*, Academic press, 2017, pp. 3-22.

[41] L. Schaeffer, "The Role of Functional Groups in Drug–Receptor Interactions," in *The Practice of Medicinal Chemistry (Fourth Edition)*, Academic Press, 2008, pp. 359-378.

[42] S. Grimme, "Density functional theory with London dispersion corrections," *WIREs Computational Molecular Science,* vol. 1, no. 2, pp. 211-228, 2011.

[43] V. Barone and M. Cossi, "Quantum Calculation of Molecular Energies and Energy Gradients in Solution by a Conductor Solvent Model," *Journal of Physical Chemistry A,* vol. 102, pp. 1995-2001, 1998.

[44] F. Ersan, E. Aktürk and S. Ciraci, "Glycine self-assembled on graphene enhances the solar absorbance performance," *Carbon,* vol. 143, p. 329, 2019.

[45] M. T. Lusk and L. D. Carr, "Nano-Engineering Defect Structures on Graphene," *Physical Review Letters,* vol. 100, p. 175503, 2008.

[46] J. Ma, D. Alfè, A. Michaelides and E. Wang, "Stone-Wales defects in graphene and other planar sp2-bonded materials," *PHYSICAL REVIEW B,* vol. 80, p. 033407, 2009.

[47] Y. Ruiz-Morales, "HOMO-LUMO Gap as an Index of Molecular Size and Structure for Polycyclic Aromatic Hydrocarbons (PAHs) and Asphaltenes: A Theoretical Study. I," *The Journal of Physical Chemistry A,* vol. 106, p. 11283, 2002.

[48] J. Kumar, Ansh and M. Shrivastava, "Stone–Wales Defect and Vacancy-Assisted Enhanced Atomic Orbital Interactions Between Graphene and Ambient Gases: A First-Principles Insight," *ACS Omega,* vol. 5, no. 48, p. 31281, 2020.

[49] M. Kamela and K. Mohammadifard, "Understanding the Interaction of glycine amino acid with graphene: An Alternative Theoretical Approach Based on Density Functional Theory," *Journal of Chemistry Letters,* vol. 1, p. 149, 2020.

[50] H.A.Duarte, "Molecular Simulation of Nanosized Tubular Clay Minerals," in *Development in clay science*, Elsevier, 2016, pp. 331-359.

[51] "Computational studies on the interactions of glycine amino acid with graphene, h-BN and h-SiC monolayers," *Physical Chemistry Chemical Physics,* vol. 3, 2017.

[52] P. Singla, M. Riyaz, S. Singhala and N. Goel, "Theoretical study of adsorption of amino acids on graphene and BN sheet in gas and aqueous phase with empirical DFT dispersion correction," *Physical Chemistry Chemical Physics,* vol. 18, pp. 5597-5604, 2016.

9. Supplementary information

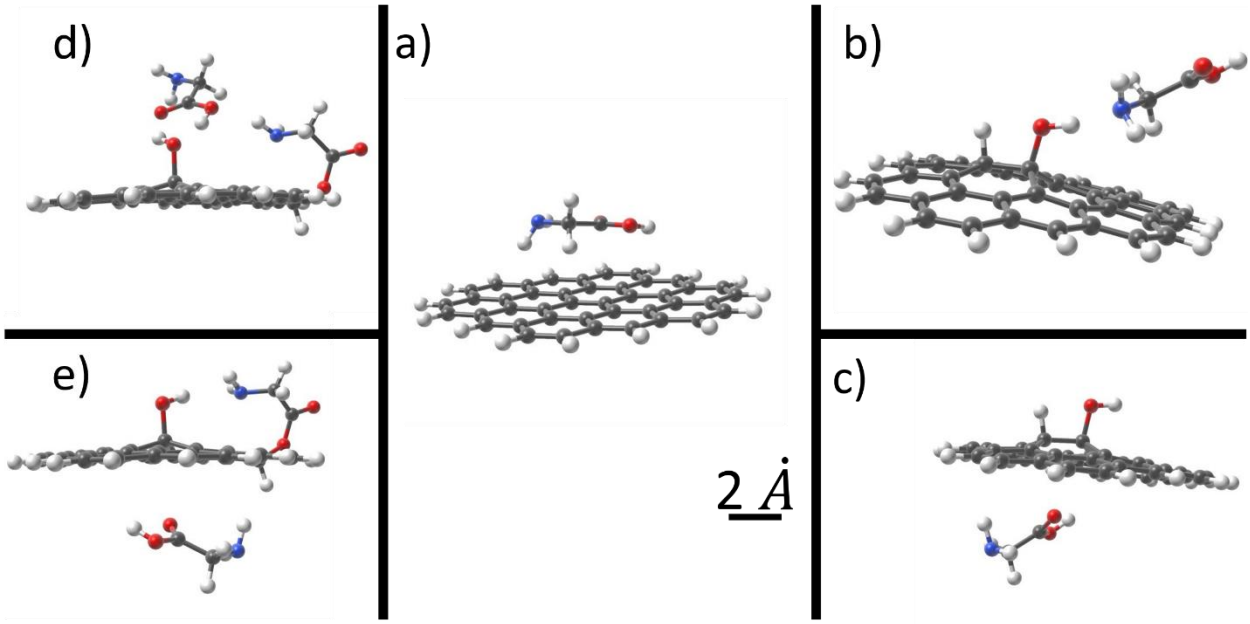

Supplementary Figure 1. Optimized structures for the non-covalent complexes formed between neutral glycine (GLY) and graphene oxide models as obtained at the RKS PBE/def2-SVP level of theory. GLY interacting with a graphene flake (a); GLY interacting with graphene oxide with hydroxyl group, GOH, from the top (b); GLY interacting with GOH from the bottom (c); GLY interacting with GOH derivatized with a glycine molecule, GOH-GLY, from the top (d); GLY interacting with GOH derivatized with a glycine molecule, GOH-GLY, from the bottom (e).

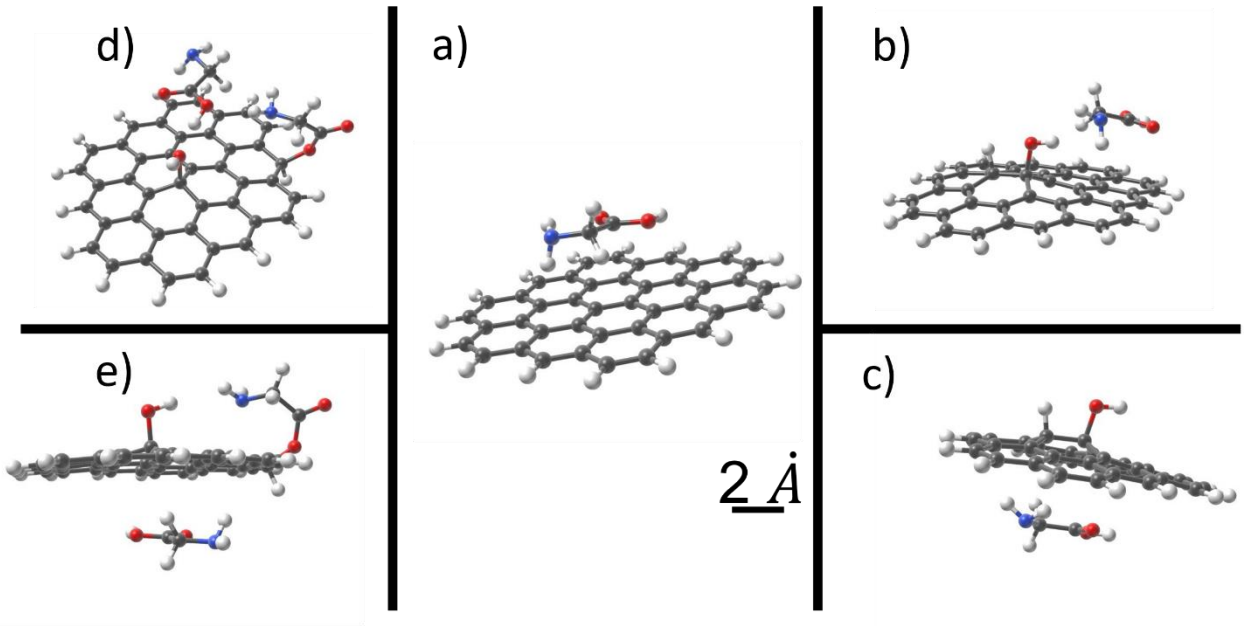

Supplementary Figure 2. Optimized structures for the non-covalent complexes formed between neutral glycine (GLY) and graphene oxide models as obtained at the RKS PBE-D3/def2-SVP by an implicit inclusion of medium (water) conducted via the conductor-like polarizable continuum model (CPCM). GLY interacting with a graphene flake (a); GLY interacting with graphene oxide with hydroxyl group, GOH, from the top (b); GLY interacting with GOH from the bottom (c); GLY interacting with GOH derivatized with a glycine molecule, GOH-GLY, from the top (d); GLY interacting with GOH derivatized with a glycine molecule, GOH-GLY, from the bottom (e).

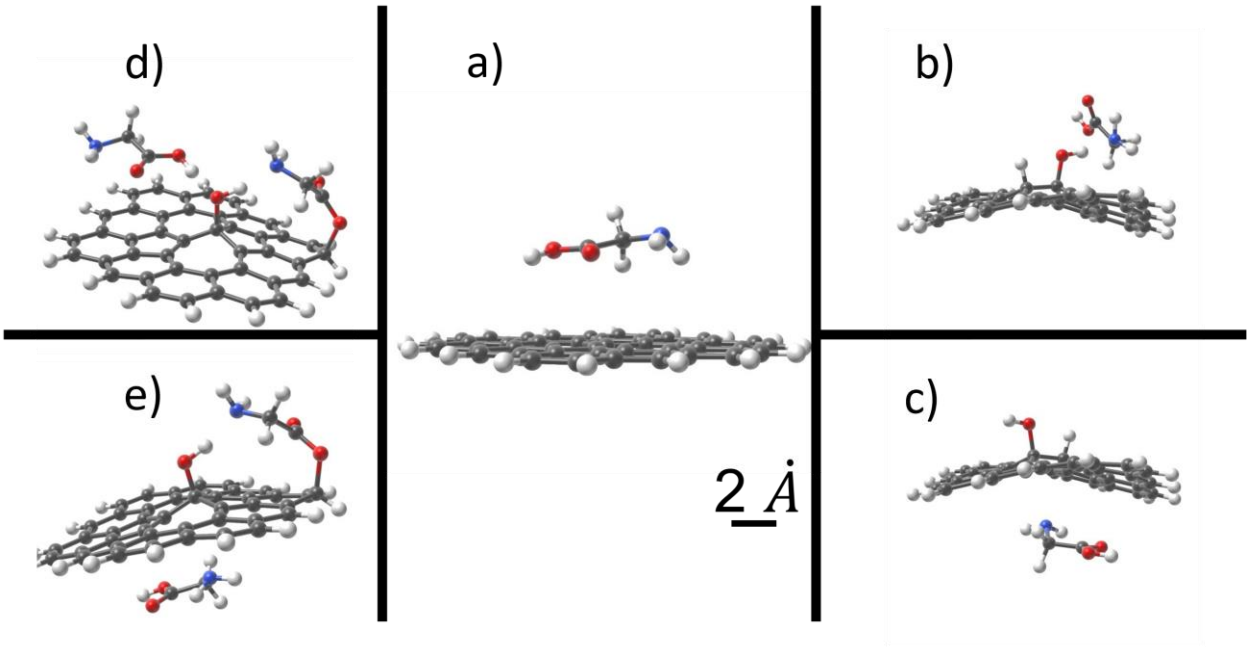

Supplementary Figure 3. Optimized structures for the non-covalent complexes formed between neutral glycine (GLY) and graphene oxide models containing Stone-Wales (SW) defects as obtained at the RKS PBE/def2-SVP level of theory. GLY interacting with a SW-graphene flake (a); GLY interacting with SW-graphene oxide with hydroxyl group, SWGOH, from the top (b); GLY interacting with SWGOH from the bottom (c); GLY interacting with SWGOH derivatized with a glycine molecule, SWGOH-GLY, from the top (d); GLY interacting with SWGOH derivatized with a glycine molecule, SWGOH-GLY, from the bottom (e).

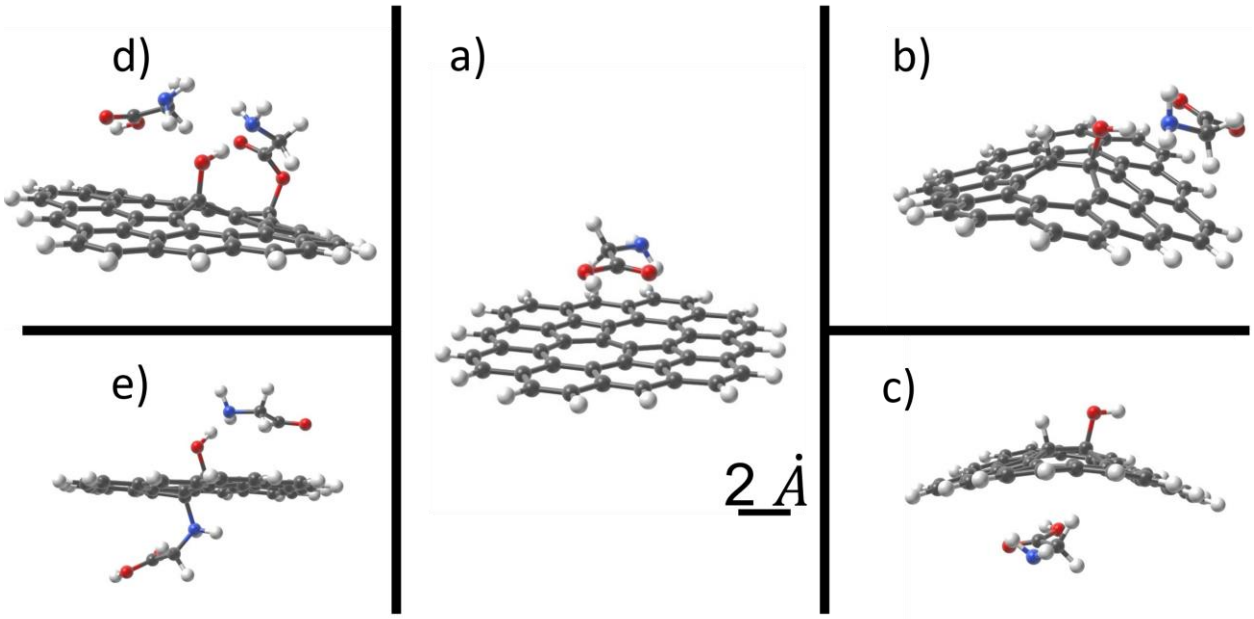

Supplementary Figure 4. Optimized structures for the non-covalent complexes formed between neutral glycine (GLY) and graphene oxide models containing Stone-Wales (SW) defects as obtained at the RKS PBE-D3/def2-SVP by an implicit inclusion of medium (water) conducted via the conductor-like polarizable continuum model (CPCM). GLY interacting with a SW-graphene flake (a); GLY interacting with SW-graphene oxide with hydroxyl group, SWGOH, from the top (b); GLY interacting with SWGOH from the bottom (c); GLY interacting with SWGOH derivatized with a glycine molecule, SWGOH-GLY, from the top (d); GLY interacting with SWGOH derivatized with a glycine molecule, SWGOH-GLY, from the bottom (e).

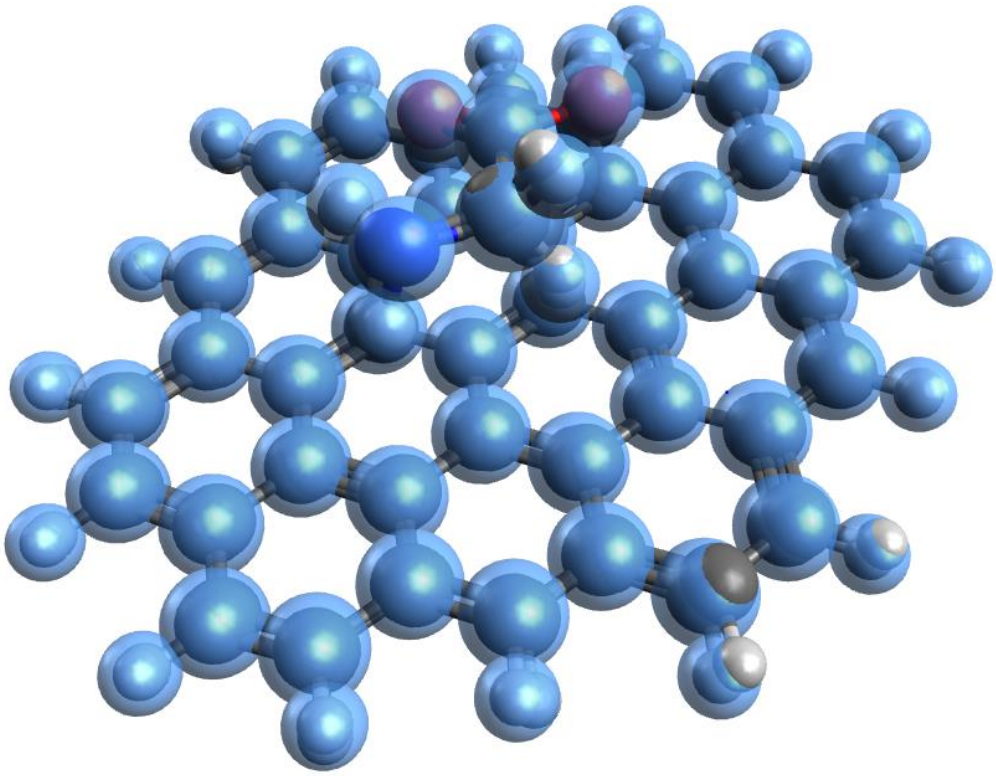

Supplementary Figure 5. Geometry configuration after 25 in the G model. Atoms encapsulated in blue, represents the final configuration of the molecule.